Photochemical & Photobiological Sciences

Accepted Manuscript

This is an *Accepted Manuscript*, which has been through the Royal Society of Chemistry peer review process and has been accepted for publication.

Accepted Manuscripts are published online shortly after acceptance, before technical editing, formatting and proof reading. Using this free service, authors can make their results available to the community, in citable form, before we publish the edited article. We will replace this *Accepted Manuscript* with the edited and formatted *Advance Article* as soon as it is available.

You can find more information about *Accepted Manuscripts* in the Information for Authors.

Please note that technical editing may introduce minor changes to the text and/or graphics, which may alter content. The journal's standard Terms & Conditions and the Ethical guidelines still apply. In no event shall the Royal Society of Chemistry be held responsible for any errors or omissions in this *Accepted Manuscript* or any consequences arising from the use of any information it contains.

ROYAL SOCIETY OF CHEMISTRY

www.rsc.org/pps

Nanostructured anatase TiO_2 densified at high pressure as advanced visible light photocatalysts

Giovanni Carini Jr.[a,*], Francesco Parrino[b], Giovanni Palmisano[a,c], Gabriele Scandura[b], Ilaria Citro[a], Giuseppe Calogero[a], Antonino Bartolotta[a], Gaetano Di Marco[a]

[a] IPCF –CNR, V.le Ferdinando Stagno d'Alcontres, 37-98158 Messina, Italy

[b] Dipartimento Energia, Ingegneria dell'Informazione e Modelli Matematici (DEIM), Università degli Studi di Palermo, Viale delle Scienze, Ed. 6, Palermo, Italy.

[c] Department of Chemical and Environmental Engineering -Institute Center for Water and Environment (iWater) - Masdar Institute of Science and Technology PO BOX 54224 Abu Dhabi (UAE)

Abstract

This study reports on characterization and photoactivity of nanostructured TiO_2 samples, which have been permanently densified under high pressures, up to 2.1 GPa. Commercial Mirkat 211 anatase has been used as benchmark sample, in order to investigate the effect of unidirectional high pressure on structural, optical and photocatalytic properties of TiO_2. Vibrational Raman spectroscopy shows that the treatment does not cause transitions among different crystalline phases of titanium dioxide. UV-vis diffuse reflectance spectra reveal that increasing pressure gives rise to a shift of the absorption onset towards higher wavelength enhancing the photoactivity under visible radiation. Samples are also photo-electrochemically characterized and tested in the gas phase with partial oxidation of ethanol to acetaldehyde under visible irradiation. Compaction up to 0.8 GPa depresses both the alcohol conversion and the aldehyde yield, while samples treated under higher pressures show enhanced characteristics of conversion compared to pristine material. Moreover, promising results in the reduction of CO_2 are also obtained under UV-visible radiation.

Keywords

Densified TiO_2; visible light photocatalyst; ethanol selective oxidation; CO_2 reduction; UV-vis spectrophotometry

*Corresponding author: Giovanni Carini, Email: gcarini@unime.it

IPCF –CNR, V.le Ferdinando Stagno d'Alcontres, 37-98158 Messina, Italy ; Tel.: +39 090 39762

1. Introduction

Heterogeneous photocatalysis is a wide-ranging technology, which can be applied in different fields, such as water[1] and air purification,[2] selective chemical transformations,[3] functionalization of materials to get self-cleaning surfaces.[4] The most relevant advantages of the involved processes reside in the environmentally friendly and cheap semiconductors used as photocatalysts, in the mild temperatures and pressures at which reactions take place and in the lack of waste resulting from the reactions.[5,6]

The most used photocatalyst is TiO_2 due to its photostability, high activity, low cost, and abundance in its anatase and rutile crystalline forms.[7-9] Moreover, it is chemically inert and can be exposed to highly oxidant reaction media due to its outstanding photocorrosion resistance. However, a key drawback for its application in all relevant areas is related to its scarce ability to absorb visible light due to a large optical band gap of 3.0 eV for rutile[10] and 3.2 eV for anatase.[11] In particular, visible light absorption is a required feature to exploit solar light radiation, thus avoiding unwelcome expenses for electric power consumption produced by light irradiation systems. Accordingly, several methods to enlarge the light absorption range of TiO_2 have been developed over last two decades.[12-16] For instance, doping with metal and nonmetal atoms is a very popular option yielding a major structural modification of TiO_2 with resulting narrowing of its band gap.[17,18] A different method to make TiO_2 as an efficient absorber of visible light involves its sensitization by means of organic dyes, widely developed not only in photocatalytic processes[19] but also in photovoltaic devices.[20-22] The latter procedure does not imply a modification of the photocatalyst band gap, while introducing a visible light-absorbing species on the TiO_2 surface. Most of the attempts to narrow the band gap of TiO_2 resulted in photocatalysts showing reduced activity due to higher recombination of photogenerated electron-hole pairs.[23] The presence of trapping states in both cation- and anion-doped titanium dioxide systems is the main source for the detrimental recombination of electron-hole pairs. Non-metal atoms (N, S, C, P and F) have been also proposed as doping agents and particular attention was given to nitrogen, since its size (similar to that of oxygen atoms) is thought to be responsible for better results in the replacement of oxygen in the crystal lattice.[17,24]

Recently, some studies have reported mainly simulations, but also some experimental results on the effect of high pressures (up to 100 GPa) applied to powdered anatase and rutile TiO_2 which give rise to a significant narrowing of its band gap.[25-27] This method does not require any doping agent to get an increase of the visible-light absorbance of semiconductors, this peculiarity being particularly distinguished with respect to the procedures usually adopted to narrow the TiO_2 band gap. Moreover, solids permanently compacted under GPa pressures may potentially represent a new class of materials because their structure can be tuned in order to get enhanced mechanical[28,29] and optical characteristics[30,31] useful for specific technological applications. Since their density may be

progressively increased up to values involving also substantial structural changes without altering the stoichiometry, they also permit to explore the mechanism of polymorphism in crystalline systems,[32,33] that is the transition from low- to high-density crystalline phases characterized by a coordination increase of structure forming ions.

The present work aims to correlate the structural and electronic properties of densified anatase TiO_2 with its activity in order to understand the influence of increasingly high pressures on semiconducting properties. The photoactivity of studied samples has been tested in the oxidative dehydrogenation of ethanol to acetaldehyde under visible light radiation.[34,35] This process is very attractive because it allows the introduction of bioethanol in many production cycles, acetaldehyde representing one of the most employed chemical commodities.[14] Some promising results are also reported concerning the photocatalytic reduction of CO_2 under UV-vis radiation.

2. Experimental

2.1. Catalysts preparation

Commercial Mirkat 211 anatase supplied by Euro Support Manufacturing was the used catalyst. Powders of TiO_2 nanoparticles were preliminarily heated at 120 °C in nitrogen atmosphere for 24 h to remove the water adsorbed on the surface. Densification of anatase TiO_2 samples was obtained by loading a small amount (≈ 500 mg) of nanoparticle powder between two pellets in a stainless steel (AISI 440c) piston-cylinder system for sintering under high uniaxial pressure ranging from 0.5 to 2.1 GPa. The piston-cylinder system was then put in a manual hydraulic press with an upper limit load of 30 tons. Compressing the powder under high pressure for 24 h at room temperature allowed to obtain samples having a cylindrical shape with a diameter of 13 mm and a height of about 1 mm.

2.2. Catalysts characterization

UV-vis absorbance spectra were recorded in diffuse reflectance mode by using an integrating sphere of a *Lambda 20 – Perkin Elmer* spectrophotometer. The measurement were performed by using permanently densified cylindrical samples or nanopowders compacted at room pressure, each sample consisting of about 500 mg of materials.

Raman spectra were obtained in backscattering configuration by a micro-Raman spectrometer Horiba Jobin-Yvon HR800, equipped with a He-Ne laser (wavelength of 632.8 nm) and a CCD Synapse detector. By using a diffraction grating having 1800/mm lines, a resolution of 0.5 cm^{-1} was obtained.

The catalysts morphology was investigated by scanning electron microscopy (SEM) performed using a FEI Quanta 200 ESEM microscope, operating at 30 kV on specimens upon which a thin layer of gold had been evaporated.

2.3. Photoanode preparation

The photoanodes consisted of a porous nanocrystalline film deposited on a FTO conductive glass (2x2 cm). The FTO glass was first degreased by an ultrasound treatment in a mixture of ethanol and water, rinsed with demineralized water, and dried at 40 °C for 30 min. The obtained cylindrical photocatalysts were then pounded in an agate mortar to obtain permanently densified nanopowder. Subsequently a suspension of 100 mg of densified nanopowder in 0.3 ml of polyethylene glycol methyl ether (PEG 550) (Sigma-Aldrich) and 0.1 ml of Triton-X100 (Sigma-Aldrich) was deposited on the FTO glass by using the Doctor blade method. The obtained film was finally calcined at 500 °C for 90 min to ensure mechanical stability. The thickness of the films ranged between 20 and 25 μm. These values were measured by means of a DektakXT profilometer (Bruker) equipped with a diamond-tipped stylus having a radius of 2 μm.

2.4. Photoelectrochemical characterization

The photoelectrochemical characterization of both pristine and permanently densified TiO_2 nanopowders was performed by a two electrodes home-made photoelectrochemical cell. Each photoanode was assembled into a sandwich type arrangement with a Pt counter-electrode sputtered on a FTO substrate, with KOH 1.0 M used as filling solution. To avoid evaporation of the electrolyte, the cells were sealed by a plastic paraffin film (parafilm) and ensured by clips.

The incident photon-to-current conversion efficiency (IPCE) and the relative photoaction spectra were measured by a IPCE station. The working electrode was irradiated from the back side by a 150 W Xenon Light Source (model ASB-XE, Spectral Products), whose emission wavelengths were selected by a monochromator (model CM110, Spectral Products) equipped with a slit set. IPCE spectra were collected between 330 and 440 nm by means of a digital Picoamperometer (model 6487, Keithley). The digital multimeter and the monochromator were simultaneously controlled by an IPCE Solarena Software.

2.5. Photocatalytic reactivity

The photocatalytic oxidation of ethanol was performed in a Pyrex batch gas-solid reactor (V = 110 mL), equipped with a silicon/teflon septum and irradiated from the top by a Solarbox (Xenon lamp of 1500 W). 1 M $NaNO_2$ aqueous solution flowing in a thimble around the reactor ensured cut-off

of 99 % UV radiation (λ < 400 nm) and hindered IR radiation to pass through producing a significant reactor overheating. The 400-950 nm radiance reaching the reactor upper surface was equal to 850 W/m^2. Reactor temperature reached a stable value of ca. 40 °C. The catalyst samples were powdered before use and then 430 mg were put into the reactor, which was firstly saturated by O_2 and then fed with 10 μL of absolute ethanol. Samples of gas (0.25 mL) were withdrawn by using gas-tight syringes at fixed time intervals.

The photocatalytic reduction of CO_2 was performed in a Pyrex batch gas-solid reactor (V=120 mL), equipped with a silicon/teflon septum and irradiated from the top by a 400 W medium pressure Hg lamp. Water was positioned between the lamp and the photoreactor to cut the infrared radiation. The 315-400 nm radiance reaching the reactor upper surface was equal to 18 W/m^2, whereas the 450-950 nm radiance was 300 W/m^2. The catalysts (200 mg) underwent a preliminary 6 h irradiation under an oxygen flow to degrade every organic surface impurities. Afterwards the batch reactor was fed by CO_2 saturated with water taking care to get rid of all oxygen traces inside the reactor. 0.5 mL of the gaseous mixture were withdrawn at fixed irradiation times by using a gas-tight microsyringe.

The evolution of ethanol, acetaldehyde and of the organic products obtained from CO_2 photocatalytic reduction was followed by a GC-2010 Shimadzu gas chromatograph equipped with a Phenomenex Zebron Wax-plus (30 m x 0.32 μm x 0.53 μm) column and a flame ionization detector, using He as carrier gas. Monitoring of CO_2 and other inorganic species was performed by means of a thermal conductivity detector installed in a Hewlett-Packard 6890 GC equipped with a 60/80 Carboxen 1000 Supelco column. The accuracy of measurements was verified by multipoint calibrations. Each experimental run was repeated twice, by achieving a maximum deviation of ca. 4 %.

3. Results and Discussion

3.1. Structural characterization

Figure 1 compares the Raman spectra of pristine anatase powders with those permanently densified at 0.7, 1.4 and 2.1 GPa. All the spectra clearly show six active optical Raman modes: 144 cm^{-1} (E_g), 197 cm^{-1} (E_g), 399 cm^{-1} (B_{1g}), 513 cm^{-1} (A_{1g}), 519 cm^{-1} (B_{1g}) and 639 cm^{-1}. These values are characteristic of the anatase phase, as reported in literature.[36] The only change observed with increasing densification is the progressive increase of band intensities, which accounts for a

growingly larger average number of particles characterizing the scattering volume. From these results, one can conclude that the materials preserve their original structure if subjected to a pressure up to 2.1 GPa.

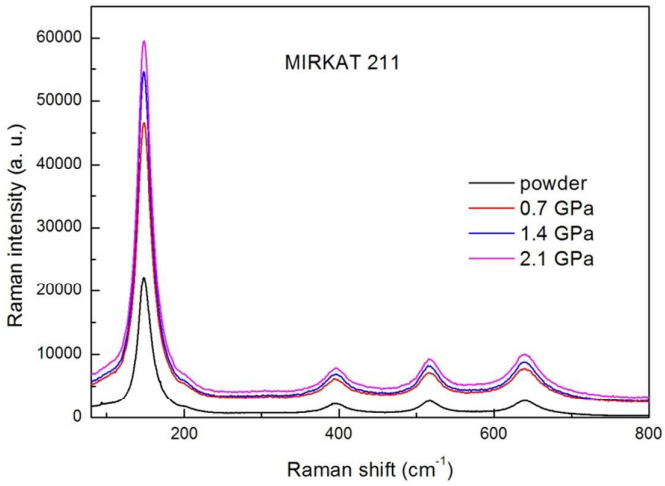

Figure 1. Raman spectra of Mirkat 211 anatase bare and densified samples.

SEM micrographs of TiO_2 nanopowders densified at 0.7, 1.4 e 2.1 GPa are reported in Figures 2a, 2b and 2c, respectively. The sample densified at 0.7 GPa is characterized by the presence of nanosized spherical agglomerates of particles separated by void regions. Upon densification at increasingly higher pressures, the nanostructures become more homogeneously distributed, the particles exhibit a lower agglomeration degree and the void regions between them become even smaller.

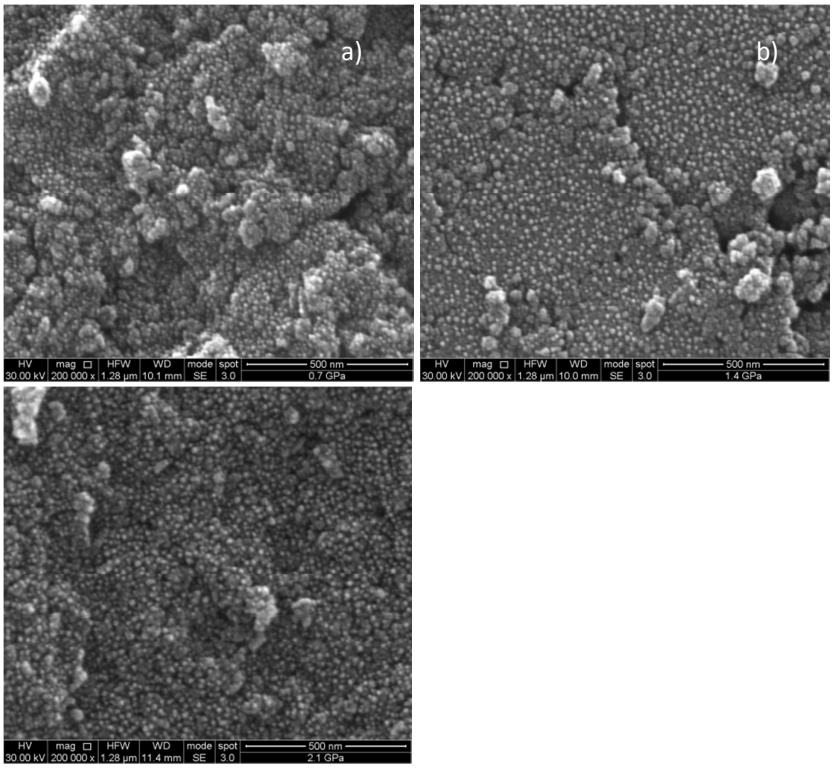

Figure 2. SEM images of Mirkat 211 densified at 0.7 (a), 1.4 (b) and 2.1 (c) GPa.

3.2. Electronic characterization

Figure 3 reports diffuse reflectance spectra of Mirkat 211 anatase, as received and permanently densified. All the spectra are characterized by a single broad band due to the charge transfer from the valence to the conduction band. Increasing sintering pressure results in a red shift of the threshold of the absorption band from 380 nm in the case of pristine sample to 391, 401 and 405 nm for samples densified at 0.7, 1.4 and 2.1 GPa, respectively. It is worth noting that the sample absorbance increases with increasing pressure in the visible region, while decreasing in the UV region. The higher absorption in the visible range can be attributed to the presence of defects due to densification process. Since the Raman spectroscopy does not evidence any structural modification or distortion of crystalline phases, the defects must be localized on the surface of nanopowders. These defects introduce intermediate energy levels between the valence and conduction bands which allow to excite electrons to higher wavelengths. Accordingly, the color of powders gradually darkens with increasing sintering pressure as shown in Figure 4. The decrease of the absorption band in UV region can be tentatively explained by hypothesizing that intermediate energy levels, localized close to the valence band, are introduced through the densification process and are acting as the highest occupied energy states. The electronic transitions from these states result statistically

favored with respect to those from the valence band, the latter being evidenced by a smaller intensity of the corresponding absorption band. As expected this behavior results more evident the higher is the extent of the introduced defects, i.e. the higher is the densification pressure.

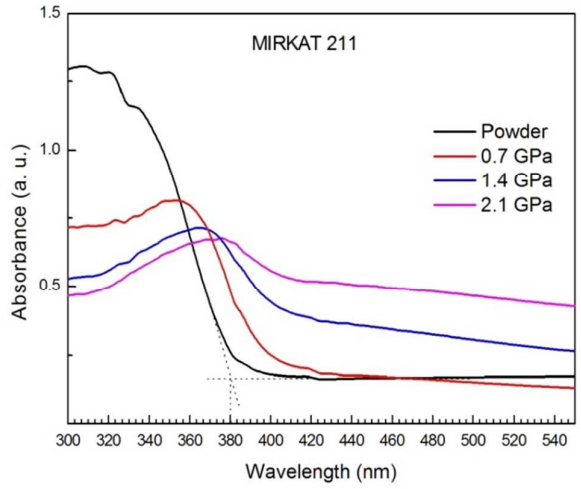

Figure 3. UV-vis diffuse reflectance spectra of bare and densified Mirkat 211 anatase.

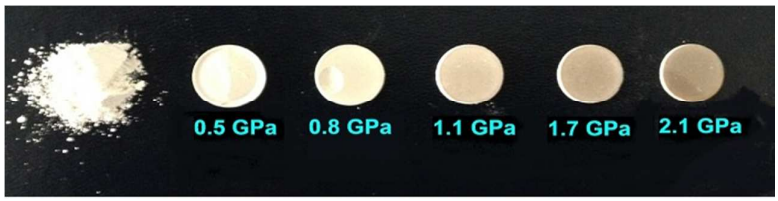

Figure 4. Digital images of bare and densified Mirkat 211 anatase.

3.3 Photoelectrochemical characterization (IPCE)

To observe the number of collected electrons per incident photons at a given irradiation wavelength we performed IPCE measurements on both pristine and permanently densified nanostructured TiO_2. IPCE vs wavelength curves were calculated from photoelectrochemical measurements according to the following equation:

$$IPCE(\%) = \left[\frac{1240 \times I_{SC}}{P_{light} \times \lambda} \right] \times 100$$

where I_{SC} and P_{ligth} are the measured short circuit photocurrent density and illumination power density at the wavelength λ of the incident light, respectively.

Figure 5a compares the photoaction spectra of normal and permanently densified (at 2.1 GPa) TiO_2 between 315 and 450 nm. Apparently, the IPCE of compacted sample is lower than that of normal sample, the latter exhibiting the same behavior observed in the absorption spectrum; but no correction was made for reflection or absorption losses from the FTO-glass which is fully absorbing for wavelengths lower than 320 nm. To account for these extrinsic background losses introducing parasitic effects, we have normalized IPCE data to the intensity of the lowest wavelength at 315 nm. As reported in Fig. 5b, the normalized IPCE of densified sample results much larger than that of normal TiO_2.

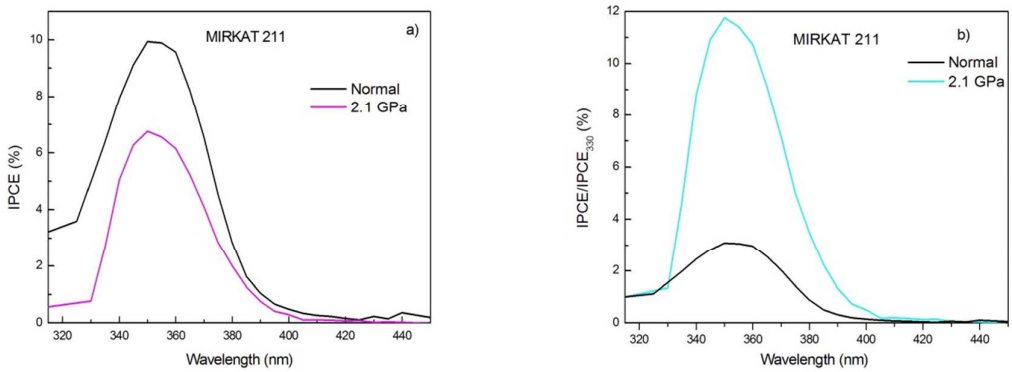

Figure 5. IPCE vs. wavelength for normal and densified anatase samples.

Even if the IPCE level increases with densification, the results do not evidence any red-shift of the TiO_2 characteristic band and a higher absorption in the visible range emphasizing the limited sensitivity of the probe.

In order to avoid questions about the possible appearance of some structural transition during sintering process at 550 °C of the photoanode, we carried out calorimetric measurements, from room temperature up to 800 °C, by differential scanning calorimetry on densified nanoparticles after the pounding process in the agata mortar. The thermograms did not show neither eso- or endo-thermal peaks nor changes of baseline.

3.4 Photocatalytic tests

Photocatalytic tests were carried out by oxidizing ethanol to acetaldehyde in gas phase in presence of pristine and densified Mirkat anatase, which is the most active allotropic phase for oxidative reactions. It is worth emphasizing that acetaldehyde is used as an important precursor to acetic acid, although nowadays this application has declined since acetic acid is more efficiently synthesized

from methanol, and to pyridine derivatives, formed by condensation, as well as of pentaerythritol and crotonaldehyde. Reaction between urea and acetaldehyde produce resins, and acetic anhydride reacts with acetaldehyde to produce ethylidene diacetate, from which vinyl acetate and finally polyvinyl acetate are obtained.[37] No reactivity was observed in absence of light, catalyst or oxygen. Figure 6 reports the concentration of acetaldehyde produced vs the irradiation time. For all the catalysts, the aldehyde concentration increases until a constant value is reached, i.e. the rate of production of aldehyde is equal to its degradation rate, and the irradiation has been stopped. Table 1 reports the results of ethanol oxidation to acetaldehyde in terms of the formation rate and the maximum amount of aldehyde produced during experiments performed in O_2 atmosphere with pristine and densified anatase. Conversions are not reported because a significant amount of ethanol is adsorbed on the catalysts surface under dark conditions, preventing to determine the global amount of converted substrate. Increasing pressure up to 0.7 GPa resulted in a decrease of both the initial formation rate and the maximum amount of aldehyde produced with respect to the pristine sample. Furthermore, samples densified at 0.5 and 0.7 GPa exhibit similar values of r_0 and the maximum aldehyde concentration. When the pressure is further increased, it is observed that both the formation rate and the maximum amount of aldehyde become higher than those of pristine anatase. Although the structure of powders does not change (see Raman spectra), densification promotes higher light absorption ability in the visible region and provides more compacted and homogeneously distributed nanoparticles (see SEM images). The optical changes are almost linearly dependent on pressure, so that the photoactivity cannot be explained only by taking into account the higher absorption ability in the visible region which might play a predominant role above 0.7 GPa. On the other hand, the morphology of the samples may constitute a key factor for understanding the reactivity trend, so that the lower activity of samples densified up to 0.7 GPa can be explained by considering the particle sintering and the reduction of the surface area. At higher pressure, however, the void regions between the particles become smaller and the electrical links between them result more efficient. Thus, the mobility of the charge carriers becomes higher reducing the exciton recombination, favoring charge and energy transfer and enhancing the photocatalytic activity. This finding can be considered as an indirect experimental evidence of the antenna effect between TiO_2 nanoparticles postulated by Wang et al.[38].

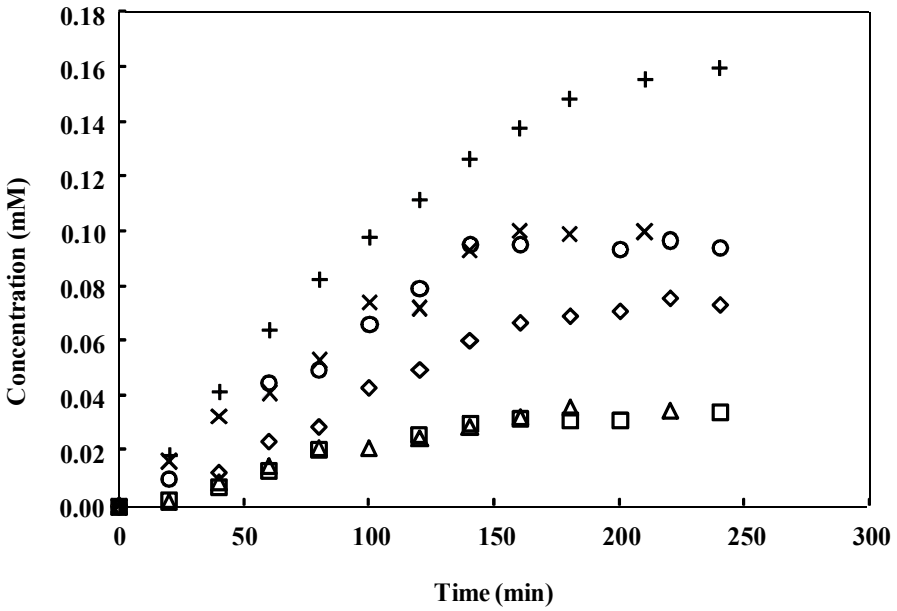

Figure 6: Time evolution of acetaldehyde concentration for partial oxidation of ethanol in gas phase carried out under visible irradiation ($\lambda \geq 400$nm) in presence of O_2 and of Mirkat anatase, pristine (◊) and densified at 0.5 GPa (□), 0.7 GPa (Δ), 1.1 GPa (○), 1.7 GPa (x) and 2.1 GPa (+).

Table 1: Formation rate of acetaldehyde and maximum acetaldehyde concentration obtained for partial oxidation of ethanol in gas phase. Runs carried out under visible irradiation ($\lambda \geq 400$nm) in presence of O_2 and of pristine and densified Mirkat anatase.

Samples	**$r_{0,\text{ acetaldehyde formation}} \cdot 10^4$ ($mM \cdot min^{-1}$)**	**Maximum acetaldehyde concentration $\cdot 10^2$ (mM)**
Mirkat	4.6	7.5
Mirkat 0.5 GPa	3.1	3.3
Mirkat 0.7 GPa	3.2	3.4
Mirkat 1.1 GPa	6.6	9.5
Mirkat 1.7 GPa	7.0	10.0
Mirkat 2.1GPa	10.8	16.0

Table 2. Photocatalytic reduction of CO_2

Catalyst	*Major reduction product*	*Major product concentration [μM]*	*Minor reduction products*	*Minor products concentration [μM]*	*Irradiation time needed [h]*
Mirkat 0.7GPa	formaldehyde	10.3	methane, ethylformate	< 0.5	2.25
Mirkat 2.1GPa	formaldehyde	5.48	methane, ethylformate	< 0.5	2.67

Table 2 reports the results of CO_2 photoreduction runs carried out in presence of Mirkat anatase densified at 0.7 and 2.1 GPa. Formaldehyde was the major reduction product whose order of magnitude is reported in μM. It is interesting to note that the figures obtained for CO_2 reduction on Mirkat densified at 0.7 and 2.1 GPa agree with the results obtained for ethanol partial oxidation. Samples compacted at 2.1 GPa were more oxidizing than those at 0.7 GPa, providing the highest amount of acetaldehyde with the highest formation rate in ethanol partial oxidation, while samples compacted at 0.7 GPa produced the highest amount of formaldehyde from CO_2 reduction.

4. Conclusions

Nanostructured TiO_2 in the anatase allotropic phase was densified at different pressures ranging between 0.5 and 2.1 GPa. Structural characterization revealed that the pressure treatment does not modify the crystalline phase, while strongly affecting the electronic structure of the samples. Increasing sintering pressure causes a red shift of the onset of absorption in UV-vis spectra of powders enhancing their visible light absorption ability.

Differently from UV-vis absorption probe, IPCE analysis, performed between 315 and 450 nm only, does not show any red shift with increasing densification, also preventing any accurate information about the mechanisms regulating the visible range for λ>450 nm because of the limited interval explored. However, IPCE data, normalized by the intensity of the lowest wavelength at 315 nm, show a substantial increase of the efficiency with sintering under high pressure.

The samples were tested in the photocatalytic partial oxidation of ethanol to acetaldehyde under visible irradiation. The sintering process depresses both the formation rate and the maximum amount produced of acetaldehyde up to 0.8 GPa. At pressures higher than 0.8 GPa the compacted samples result more active than the pristine one. Densified samples were also tested for CO_2 photocatalytic reduction in gas phase producing mainly formaldehyde with amounts of 10.3 μM and

5.48 μM for samples densified at 0.7 and 2.1 GPa respectively . The production increase observed in densified samples over the visible range is ascribed to structural defects induced by high pressure sintering.

ACKNOWLEDGMENTS

We gratefully acknowledge PON– Industria 2007-2013: Progetto FotoRiduCO2 (prot. PON01_02257), ENERGETIC (prot. PON02_00355_3391233) and TESEO (prot. PON02_00153_2939517). Furthermore this research was supported by "CNR-EFOR" Project and by Project "SAGRO" supported by Regione Siciliana (PO-FESR 2007/2013 linea d'intervento 4.1.1.1).

We also thank Prof. Fortunato Neri and Francesco Barreca for SEM images, Cristiano D'Andrea for Raman measurements and Daniele Cosio for his technical assistance.

REFERENCES

1. A. Sobczynski and A. Dobosz, Water Purification by Photocatalysis on Semiconductors, *Polish J. of Environmental Studies,* 2001, **10**(4), 195-205.
2. J. Peral, X. Domènech and D. F. Ollis, Heterogeneous Photocatalysis for Purification, Decontamination and Deodorization of Air, *J. of Chem. Technol. and Biotechnol.*, 1997, **70**, 117-140.
3. G. Palmisano, V. Augugliaro, M. Pagliaro and L. Palmisano, Photocatalysis: a promising route for 21st century organic chemistry, *Chem. Commun.,* 2007, 3425-3437.
4. A. Fujishima, X. Zhang and D. A. Trykc, TiO2 photocatalysis and related surface phenomena, *Surface Science Reports,* 2008, **63**, 515-582.
5. A. O. Ibhadon and P. Fitzpatrick, Heterogeneous Photocatalysis: Recent Advances and Applications, *Catalysts,* 2013, **3**, 189-218.
6. M. N. Chong, B. Jin, C. W. K. Chow and C. Saint, Recent developments in photocatalytic water treatment technology: A review, *Water Research,* 2010, **44**, 2997-3027.
7. A. Mills and S. Le Hunte, An overview of semiconductor photocatalysis, *J. of Photochem. and Photobiol. A: Chemistry,* 1997, **108**, 1-35

8. A. L. Linsebigler, G. Q. Lu and J. T. Yates, Photocatalysis on TiO_2 Surfaces: Principles, Mechanisms, and Selected Results, *Chem. Rev.,* 1995, **95**, 735-758.

9. M. R. Hoffmann, S. T. Martin, W. Choi and D. W. Bahnemann, Environmental Applications of Semiconductor photocatalysis, *Chem. Rev.,* 1995, **95**, 69-96.

10. A. Amtout and R. Leonelli, Optical properties of rutile near its fundamental band gap, *Phys. Rev. B,* 1995, **51**, 6842-6851.

11. H. Tang, H. Berger, P. E. Schmid and F. Levy, Photoluminescence in TiO_2 anatase single crystals, *Solid State Commun.,* 1993, **87**(9), 847-850.

12. G. Mele, G. Ciccarella, G. Vasapollo, E. García-López, L. Palmisano and M. Schiavello, *Applied Catalysis B: Environmental,* 2002, **38**, 309-319.

13. W. J. Youngblood, S.-H. A. Lee, K. Maeda and T. E. Mallouk, Visible Light Water Splitting Using Dye-Sensitized Oxide Semiconductors, *Accounts Of Chemical Research*, 2009, **42**(12), 1966-1973.

14. G. Qin, Z. Sun, Q. Wu, L. Lin, M. Liang and S. Xue, Dye-Sensitized TiO2 film with bifunctionalized zones for photocatalytic degradation of 4-cholophenol, *J. of Hazardous Materials,* 2011, **192**(2), 599–604.

15. F. Parrino, V. Augugliaro, G. Camera-Roda, V. Loddo, M. J. López-Muñoz, C. Márquez-Álvarez, G. Palmisano, L. Palmisano and M. A. Puma, Visible-light-induced oxidation of *trans*-ferulic acid by TiO_2 photocatalysis, *J. Catal.,* 2012, **295**, 254-260.

16. F. Parrino, A. Ramakrishnan, C. Damm and H. Kisch, Visible-Light-Induced Sulfoxidation of Alkanes in the Presence of Titania, *ChemPlusChem.,* 2012, **77** (8), 713-720.

17. A. Zaleska, Doped-TiO2: A Review, *Recent Patents on Engineering,* 2008, **2**, 157-164.

18. Z. M. Dai, G. Burgeth, F. Parrino and H. Kisch, Visible light photocatalysis by a Titania-Rhodium(III) complex, *J. Organomet. Chem.,* 2008, **694**, 1049-1054.

19. C. Guarisco, G. Palmisano, G. Calogero, R. Ciriminna, G. Di Marco, V. Loddo, M. Pagliaro and F. Parrino, *Photocatalysis: New Highlights From Jep. 2013,* 2014**,** DOI 10.1007/s11356-014-2546-z.

20. G. Calogero, A. Sinopoli, I. Citro, G. Di Marco, V. Petrov, A. M. Diniz, A. J. Parola and F. Pina, Synthetic analogues of anthocyanins as sensitizers for dye-sensitized solar cells, *Photochem. Photobiol. Sci.*, 2013, **12**, 883-894.

21. G. Calogero, I. Citro, G. Di Marco, S. A. Minicante, M. Morabito, G. Genovese and Brown seaweed pigment as a dye source for photoelectrochemical solar cells, *Spectrochimica Acta Part A: Molecular and Biomolecular Spectroscopy,* 2014, **117,** 702–706.

22. G. Calogero, I. Citro, C. Crupi and G. Di Marco, Absorption spectra and photovoltaic characterization of chlorophyllins as sensitizers for dye-sensitized solar cells, *Spectrochimica Acta Part A: Molecular and Biomolecular Spectroscopy,* 2014, **132**, 477–484.

23. B. Ohtani, Titania photocatalysis beyond recombination: a critical review, *Catalysts,* 2013, **3**, 942-953.

24. T.-H. Xu, C.-L. Song, Y. Liu and G.-R. Han, Band structures of TiO_2 doped with N, C and B, *J. Zhejiang Univ Sci B.,* 2006, 7(4), 299–303.

25. M. Mattesini, J. S. Almeida, L. Dubrovinsky, N. Dubrovinskaia, B. Johansson and R. Ahuja, Cubic TiO_2 as a potential light absorber in solar-energy conversion, *Phys. Rev. B,* 2004, **70**, 115101-115109.

26. T. Mahmood, C. Cao, W. S. Khan, Z. Usman, F. K. Butt and S. Hussain, Electronic, elastic, optical properties of rutile TiO2 under pressure: a DFT study, *Physica B*, 2012, **407,** 958-965.

27. T. Mahmood, C. Cao, R. Ahmed, M. Ahmed, M. A. Saeed, A. A. Zafar, T. Husain and M. A. Kamran, Pressure induced structural and electronic bandgap properties of anatase and rutile TiO_2, *Sains Malaysiana,* 2013, **42**(2), 231-237.

28. G. Carini Jr, G. Carini, G. Tripodo, G. Di Marco and E. Gilioli, Elastic and anelastic properties of densified vitreous B_2O_3: Relaxations and anharmonicity, *Phys. Rev. B*, 2012, **85** (9), 094201 (8).

29. C. S. Zha, R. J. Hemley, H. K. Mao, T. S. Duffy and C. Meade, Acoustic velocities and refractive index of SiO2 glass to 57.5 GPa by Brillouin scattering, *Phys. Rev. B*, 1994, **50**(18), 13105-13112.

30. N. Soga, K. Hirao, M. Yoshimoto and H, Yamamoto, Effects of densification on fluorescence spectra and glass structure of Eu3+ doped borate glasses, *J. Appl. Phys.,* 1988, **63**(9), 4451-4454.

31. M. J. Lochhead and K. L. Bray, High-pressure fluorescence line narrowing of Eu(III)-doped sodium disilicate glass, *Phys. Rev. B*, 1995, **52**(22), 15763-15775.

32. R. J. Hemley, Pressure dependence of Raman spectra of SiO_2 polimorphs: α-quartz, coesite, and stishovite, in *High-pressure Research in Mineral Physics*, edited by M.H. Manghnani and Y. Syono, (Terra Scientific Publishing Company, Tokyo, 1987), pp. 347-359.

33. B. Wehinger, A. Bosak, A. Chumakov, A. Mirone, B. Winkler, L. Dubrovinsky, N. Dubrovinskaia, V. Brazhkin, T. Dyuzheva and M. Krisch, Lattice dynamics of coesite, *J. Physics: Condens. Matter*, 2013, **25**, 275401 (8).

34. Y. Gucbilmez, T. Dogu and S. Balci, Ethylene and acetaldehyde production by selective oxidation of ethanol using mesoporous V-MCM-41 catalysts, *Ind. Eng. Chem. Res,* 2006, **45**, 3496-3502.

35. K. Yu. Koltunov and V. I. Sobolev, Selective gas-phase oxidation of ethanol by molecular oxygen over oxide and gold-containing catalysts, *Catal. Ind*., 2012, **4,** 247-252.

36. T. Ohsaka, Temperature dependence of the Raman spectrum in anatase TiO_2, *J. Phys. Soc. Jpn.,* 1980, **48**(5), 1661-1668.

37. M. Eckert, G. Fleischmann, R. Jira, H. M. Bolt and K. Golka, Acetaldehyde, *Ullmann's Encyclopedia Of Industrial Chemistry*, 2006, doi:10.1002/14356007.a01_031.pub2.

38. C. Wang, C. Böttcher, D. W. Bahnemann and J. K. Dohrmann, *J. Nanoparticles Research* 2004, **6**, 119-122.

Graphical and textual abstract

Uniaxial high pressure up to 2.1 GPa on anatase TiO_2 nanopowders induces structural defects, increases visible light absorption and enhances acethaldeide production.